**Master of Medicine**

# Development of an Automatic Segmentation System for Anterolateral Thigh Flap Perforators in Maxillofacial Reconstruction

**The Graduate School**
**of the University of Ulsan**

**Department of Medicine**
**Ji-Su Oh**

# Development of an Automatic Segmentation System for Anterolateral Thigh Flap Perforators in Maxillofacial Reconstruction

**Supervisor: Jee-Ho Lee DDS MSD PhD**

**A dissertation**

**Submitted to**
**Graduate School of University of Ulsan**
**In partial Fulfillment of the Requirements**
**for the Degree of**

**Master of Medicine**

**By**

**Ji-Su Oh**

**Department of Medicine**
**University of Ulsan, Korea**
**February 2024**

# Development of an Automatic Segmentation System for Anterolateral Thigh Flap Perforators in Maxillofacial Reconstruction

**This certifies that the dissertation/master thesis of Ji-Su Oh is approved.**

**Bu-Kyu Lee**
**Committee Vice-chair Dr.**
**Jee-Ho Lee**
**Committee Member Dr.**
**In-Seok Song**
**Committee Member Dr.**

**Department of Medicine**
**University of Ulsan, Korea**
**February 2024**

**English abstract**

# Development of an Automatic Segmentation System for Anterolateral Thigh Flap Perforators in Maxillofacial Reconstruction

**Ji-Su Oh, D.D.S**

**Directed by Jee-Ho Lee, D.D.S., M.S.D., PhD**

**Department of Dentistry, Graduate school of Medicine, University of Ulsan**

**Introduction**

The anterolateral thigh (ALT) flap is one of the most preferred flaps for maxillofacial reconstruction and for finding a skin perforator in an important first step in flap design. Computed tomography angiography (CTA) can be used through image mapping, contributing to the establishment of an appropriate flap design plan and reducing surgical time. However, preoperative mapping is time-consuming and can be affected by the image quality and clinician's skill. This study aimed to develop an automatic segmentation system for ALT flap perforators using a convolutional neural network in CTA and evaluate its efficiency and accuracy.

**Material & Methods**

This study enrolled 80 patients who underwent CTA for maxillofacial reconstruction. A single researcher performed mapping of bilateral lateral femoral circumflex artery perforators on uploaded CTA using AVIEW Modeler (version 1.1.42.7, Coreline Software, Seoul, Korea). Training for the

development of automatic segmentation system was conducted using DeepLabv2 and 3D ResNet152. Dice Similarity Coefficient (DSC) and Jaccard Similarity Coefficient (JSC) values were calculated, and the distance difference between two points was measured. Furthermore, quadrant distribution analysis was conducted.

**Results**

As a result of the training, the DSC and JSC values were 69.67 ± 1.48 and 67.81 ± 1.70, respectively. The test results for the 13 dataset were DSC with 69.34 ± 0.83 and JSC with 67.47 ± 0.96. The distance difference between manual and automatic detection was 38.28 ± 15.52 mm on the left side and 31.96 ± 18.11 mm on the right side. Quadrant distribution was most prevalent in the distosuperior area.

**Conclusion**

The reasonable results indicate that the automatic segmentation system for ALT flap perforator has potential for clinical application.

Keywords: Anterolateral thigh flap, Perforator flap, Automatic segmentation, Image mapping

# Contents

# List of tables



# List of figures

# Introduction

In 1984, Song et al. first introduced the anterolateral thigh (ALT) flap as a septocutaneous vessel-based flap progressing between the rectus femoris and vastus lateralis muscles.[1)] Since then, ALT flap has become one of the most preferred and versatile flap options with numerous advantages for maxillofacial reconstruction.[2)] The advantages of free flap surgery include long pedicle length with sufficient vessel diameter, various flap designs, and reduced morbidity of the donor site.[2-4)] Based on these benefits, the ALT flap has become a workhorse flap for soft tissue reconstruction.[5)]

Previous studies with cadaver and image have shown significant variations of the ALT perforator anatomy in its origin, location, and course.[6-8)] Up to 75% of ALT flap perforators originate from the descending branch of the lateral circumflex femoral artery, the largest branch of the profunda femoris, and up to 25% from the transverse branch.[2, 5, 6)] These perforators can also be found on the ascending and lateral branches of the lateral circumflex femoral artery.[9)] The progression of perforators can be categorized as septocutaneous or musculocutaneous; in the previous study, more than 85% of cases exhibited a musculocutaneous course.[2, 8-10)] The anatomical variability of ALT flap perforators poses challenges in preoperative planning, including the flap design.

Color Doppler ultrasound (CDU) and computed tomography angiography (CTA) are the most common techniques for preoperative perforator detection. CDU provides information on the flow pattern of vessels and tissue characteristics with relatively cheaper and faster accessibility and, with its portability, enables flap monitoring during the intra- and postoperative periods.[11, 12)] However, an important drawback of CDU is the steep learning curve for skilled usage and interobserver variability.[11, 13)] CTA, on the other hand, is mainly used for the detection of preoperative flap perforators through image mapping with improved sensitivity and specificity, contributing to the establishment of an appropriate flap design plan; however, preoperative mapping on CTA is time-consuming, depending on the skill of the clinician, and is affected by the quality of images.[14)] Muscle regions in CTA usually exhibit high radiodensity, making it difficult for clinicians to identify

perforators that progress through intramuscular regions.[15] Furthermore, flap perforator mapping is quite subjective, resulting in incoherences between preoperative mapping and surgical findings; this may lead to the possibility of intraoperative modification of surgical planning.[16]

Considering the limitations of these diagnostic tools, deep learning and automatic detection have been introduced to assess diabetic retinopathy by analyzing fundus images or to detect nodules in the lung using computerized tomography scans.[17, 18] Previous studies have also suggested the use of automatic segmentation for effective preoperative detection of flap perforator in breast reconstruction.[15, 16] However, thorough examination of relevant literature revealed that automatic segmentation for ALT flap perforators has not yet been studied.

This study aimed to develop an automatic segmentation system for the detection of ALT flap perforators, a critical component in maxillofacial reconstruction. An experienced clinician prepared the ground truth through manual CTA mapping. Then, machine learning on segmentation using 2D and 3D images was performed. Subsequently, retrospective verification was performed on the validation datasets to compare the difference in the location of the ALT flap perforators, evaluating clinical applicability.

# Materials and Methods

The study protocol was approved by the Institutional Review Board of Asan Medical Center (IRB No. 2023-1372).

### 1. Study subjects and data collection

This study enrolled 80 patients who underwent preoperative CTA for maxillofacial reconstruction at the Department of Oral and Maxillofacial Surgery, Asan Medical Center between 1 March 2021 and 30 June 2023. The exclusion criteria were (1) patients with missing CTA data (n = 4), (2) patients in whom the collected CTA did not run on the mapping program (n = 5), and (3) patients

who had poor quality of CTA with artifacts (n = 2). The application of these criteria in this study led to the inclusion of 56 patients for training and validation and 13 patients for testing, respectively.

**2. Manual mapping of ALT flap perforator**

A single experienced clinician performed ALT flap perforator mapping using AVIEW Modeler (version 1.1.42.7, Coreline Software, Seoul, Korea). After uploading anonymized CTAs to the mapping program, the 3-mm cut of the CTA was converted to 1-mm cut using an image conversion option to accurately predict the ALT flap perforator. Manual mapping of the lateral circumflex femoral artery perforator was continuously performed without cutoff segmentation starting from the femoral artery near the hip joint to the end of the perforator that reaches the thigh skin (Fig. 1). This manual mapping served as the ground truth for the subsequent training of the automatic mapping system. The progression of the perforator was categorized as septocutaneous or musculocutaneous (Fig. 2). Each of the CTA scans from 56 patients was divided into left and right halves, thereby eliminating the distinction between sides. This approach effectively doubled our dataset, which led to the creation of 112 usable images for a more comprehensive analysis. Then, the expanded dataset was strategically divided into three subsets, training, validation, and testing, at a ratio of 8:1:1. Subsequently, to further enhance the robustness of our model testing, additional 13 scans were included in the test set.

**3. Network architectures**

This study employed a cascaded approach for the detection and segmentation of the perforators.[19, 20] The first stage of the process involved the use of DeepLabv2, a convolutional neural network known for its efficiency in semantic image segmentation.[21] Complete 2D CTA images were introduced into this network, and their original resolution of 512 × 512 pixels was maintained to preserve details important for accurate detection. The learning rate was meticulously calibrated to 0.0001 to achieve a balanced compromise between rapid convergence and avoidance of the risk of

overshooting the minimum during training. After the assessment, a batch size of 16 was selected and the DeepLabv2 model was subjected to extensive training, spanning 500 trials to fine-tune its performance.

After completing the 2D detection phase, the second stage involving 3D segmentation was initiated. In this stage, 3D patches centered on the previously detected perforator regions were extracted. These patches were 64 × 64 × 64 voxels in size; this size was selected as it was computationally manageable in the 3D ResNet152 model while still sufficiently showing the perforation regions in detail for effective segmentation. The patches were then entered into the 3D ResNet152 model for volume data learning, and network-wide recorrected linear unit activation was used, known as the efficiency of deep learning models.[22, 23] The model learning rate was set to 0.001, striking a balance between training speed and accuracy. Despite the computational complexity of 3D image processing, the patch sizes were small and numerous; thus, a batch size of 32 was selected. To ensure extensive learning while preventing overfitting, the training was conducted over a span of 300 epochs. Furthermore, several data augmentation techniques were implemented during the training process to enhance the dataset and boost the generalization capability of the model. First, rotation was applied to the scans, with random angles of up to 20°, to emulate different anatomical orientations. Second, scaling was performed, in which the size of the images was randomly varied between 90% and 110% of their original dimensions, addressing variations in anatomical structure sizes. Third, random translations were introduced in both horizontal and vertical directions to the images, with the aim of replicating positional differences. Lastly, to mimic the variability in image quality typically seen in clinical settings, the brightness and contrast of the scans were randomly adjusted.

**4. Training evaluation**

Two statistical metrics were mainly used in the evaluation of the performance of our segmentation model: Dice Similarity Coefficient (DSC) and Jaccard Similarity Coefficient (JSC).[24]

The DSC, a measure ranging from 0 to 1, quantifies the overlap between two samples, where

1 denotes perfect overlap and 0 no overlap at all. It is calculated as follows:

$$\frac{2 \times |A \cap B|}{|A| + |B|}$$

where A and B denote the actual and predicted regions, respectively.

The JSC also evaluates similarity with values between 0 and 1, but it measures the proportion of overlap to the total size of the combined samples. It is calculated as follows:

$$\frac{|A \cap B|}{|A \cup B|}$$

**5. Clinical evaluation**

The same clinician performed additional manual mapping on the datasets from 13 patients after automatic segmentation for testing. Subsequently, the results of the automatic mapping were additionally uploaded to the existing dataset with the same header value on the mapping program. The results of both automatic and manual segmentations were superimposed on the 3D image. The threshold value of the image was adjusted so that the terminal part of the perforator appeared as point on the patient's thigh skin (Fig. 3). The difference in the coordinate values between manually and automatically detected perforator points was calculated. Based on the manual detection of the flap perforator, the location of the automatic detection was divided into quadrants: mediosuperior, medioinferior, distosuperior, and distoinferior.

**6. Statistical analysis**

SPSS version 22.0 (IBM, Chicago, IL, USA) was used to conduct statistical analysis, using a significance level of $p < 0.05$. Mann-Whitney u-test was performed to compare differences in DSC and JSC values according to gender, left and right thighs, and the progression type of perforators. Additionally, Kruskal-Wallis test was performed to compare differences according to body mass index (BMI). BMI was classified based on the World

Health Organization's cutoffs: underweight (<18.5 kg/m2), healthy weight (18.5–24.99 kg/m2), overweight (25–29.99 kg/m2), or obese (≥30 kg). /m2).[25)]

# Results

### 1. Subject distribution

The datasets for the gold standard consisted of 26 men and 30 women (average age, 68.1 ± 9.6 years) for training and validation. The datasets for the test included 10 men and 3 women (average age, 61.38 ± 13.07 years). The progression type of the perforator was determined according to sex. In the training dataset, 74.1% of septocutaneous and 25.9% of musculocutaneous perforators were investigated in men and 41.4% of septocutaneous and 58.6% of musculocutaneous perforators in women (Table 1).

### 2. Training evaluation

In this study, the ALT flap perforator starting from the femoral artery near the hip joint, passing through the lateral circumflex femoral artery and reaching the thigh skin, was detected via automatic segmentation (Fig. 4). The validity of automatic segmentation for the lateral circumflex femoral artery perforator was examined using DeepLabv2 on 2D CTA and 3D ResNet152 on 3D CTA. The average DSC and JSC values were 69.67 ± 1.48 and 67.81 ± 1.70 for the training and validation datasets and 69.34 ± 0.83 and 67.47 ± 0.96 for the test datasets, respectively (Table 2).

When analyzing the DSC and JSC values according to the left and right sides of the thigh, the DSC values were 69.73 ± 1.64 for the left side and 67.82 ± 1.58 for the right side ($p = 0.005$) and the JSC values were 68.95 ± 1.69 for the left side and 67.14 ± 1.89 for the right side($p = 0.026$), which showed a higher degree of accuracy with the automatic segmentation on the left side. On the other hands, there were no statistical differences in DSC and JSC values according to gender, perforator progression type, and BMI (Table 3).

**3. Clinical evaluation**

In manual and automatic detection, 2 points of perforators reaching to the thigh skin were superimposed and the position difference was calculated. The average difference on the right side was 31.96 ± 18.11 mm, whereas the average difference on the left side was 38.28 ± 15.52 mm. The quadrants distribution of the automatic detection based on the manual detection were presented in Figure 5. The quadrants where automatic detection was most distributed was distosuperior, whereas the least distribution was mesioinferior.

# Discussion

Preoperative image detection of the perforator with CTA has been increasingly employed as a practicable adjunct for planning the ALT flap design.[14] However, the anatomical variability of vascular course in the ALT flap perforator may hinder the intraoperative process. This may cause prolonged flap harvest time, change the flap design plan, or even necessitate alteration of the flap harvest site to the contralateral leg, directly affecting the morbidity of the donor site. Previous studies demonstrated that about 3% to 5% of patients failed to find a suitable flap perforator, thus converting to an alternative flap design.[7, 26] Therefore, increased accuracy of preoperative perforator detection plays a pivotal role in long-term prognosis.

In this study, an automatic flap perforator segmentation system was developed through machine learning with the convolutional neural network to overcome the limitations of manual preoperative perforator detection using CTA, which is time-consuming and operator-dependent. The accuracy and clinical applicability of this system was also evaluated. The mIoU unit was used as the evaluation standard for automatic perforator segmentation. This percentage value is 1 if there is a perfect match by overlapping the gold standard and prediction values and 0 if there is no overlapped area at all.[27, 28] However, due to the lack of an objective indicator of prediction accuracy, a score

between 0.7 and 0.8 is regarded as reasonable for clinical applicability. In this study, the average scores ranged from 0.6750 to 0.7065 in DSC and from 0.6614 to 0.6882 in JSC, which might be acceptable levels.

In manual flap perforator mapping, the vascular course was classified into musculocutaneous or septocutaneous. Previous studies have reported that 17% to 85% of cases have musculocutaneous vascular courses.[2, 4, 8-10] Furthermore, some studies have demonstrated that the flap harvest time is delayed when the perforator goes through the vastus lateralis as musculocutaneous, which increases the morbidity of the donor site.[2, 3, 5] In this study, 56.5% and 43.5% of the patients had septocutaneous and musculocutaneous courses, respectively. The septocutaneous course was predominant in men (70.3%), whereas the musculocutaneous course was prevalent in women (59.4%). Regarding the high radiodensity in muscular areas in CTA, it can be deduced that musculocutaneous perforator detection is an operator-dependent result.[15] In manual segmentation of this study, the most difficult part to detect was the case where the perforator traveled through the muscles before proceeding to the subcutaneous area.

Each subject had varying physical and demographic characteristics, such as age, sex, muscular density, and thickness of the subcutaneous tissue. This may affect the detection accuracy and the time required for manual segmentation. In manual detection of this study, the progression course of the artery could be confirmed more clearly in younger women with sufficient subcutaneous tissue thickness in some degree and without myolysis. A previous study reported that there was no difference in the number of perforators between the dominant and nondominant legs during the ALT flap perforator detection and that it was not affected by the thickness of the subcutaneous tissue and muscle.[29] When statistical analysis was performed on the test datasets, the accuracy of the left thigh between the manual and automatic segmentation was significantly higher than that of the right thigh. On the other hand, there was no statistical difference in accuracy depending on the type of perforator progression, which was classified as septocutaneous or musculocutaneous, and gender. Additionally, no differences were identified depending on BMI index, considered to be related to the subcutaneous

tissue.

To expand into the area of computer-aided diagnosis using artificial intelligence and deep learning, it is important to understand the concepts of image classification, segmentation, and detection. Image classification regards each image as a single unit and distinguishes it from others, whereas image segmentation regards pixel points as basis, separating the image into several specific areas with its exclusive properties, including segmentation of the image with the precise boundary of the existing target. On the other hand, image detection is based on the retrieval of a given sub-image from a known image. The difference between detection and classification is that the former retrieves multiple objects in an image.[30-32] If the required level of the perforator prediction is presence or absence, detection or classification can be employed. However, image segmentation considering boundaries of images was adopted in our study as the exact location of the perforator had to be confirmed.

Our study initially conducted deep learning using DeepLabv2 with 2D images. In fact, the mIoU values for the analysis using 2D images were slightly higher than those for the analysis using 3D images. However, in the process of converting CTA from 3- to 1-mm cuts, the number of slices on average increased to more than 1000, and the image segmentation loss was partially detected. As false positives were likely to be increased in these circumstances, evaluation of overall connectivity using 3D ResNet152 with 3D images was attempted. A previous study demonstrated that 2D image segmentation was more effective than 3D image segmentation using abdominal CT images.[33] Other studies conducted segmentation using 2D and 3D images interactively. Similarly, our study used 2D and 3D images in a cascaded manner to compensate for the strengths and weaknesses of each images.[34-36]

The main trunk starting from the femoral artery near the hip joint had a large diameter, showing high agreement with manual and automatic detections, but as it went toward the terminal branches reaching the skin, a relatively disconnected area occurred in the middle area of the artery compared with the ground truth. However, because detection of perforators terminating the thigh skin

is crucial in actual intraoperative procedures, the discontinuity of the middle parts of the artery may not be a critical problem in the clinical application of the automatic perforator segmentation system.

The ABC system was introduced to detect the dominant ALT flap perforators based on the vascular characteristics of the lower limbs of Western populations. In this previous study, 89% of reliable perforators were detected 3 cm lateral to the midpoint of the line between the anterior superior iliac spine and the superior lateral corner of the patella, referred to as the A-P line.[37] When test datasets were retrospectively evaluated, all 26 ALT flap perforators were located lateral to the A-P line.

For clinical evaluation, the perforator that terminated on the thigh skin was shown as a point and the distance difference between the manual and automatic detections was calculated. There was no significant difference between the values between the left and right sides with 38.28 ± 15.52 mm and 31.96 ± 18.11 mm, respectively. The deviation was slightly high for both thighs, and in relation to this, it is believed that further research is needed on the relationship with gender, age, and perforator cousre. In addition, when the distribution of the automatic detection was classified into quadrants based on the manual detection, the distosuperior area was most frequently identified. It is expected that reproducible and stable flap harvesting would be possible if the distance difference and location of the perforator's skin terminal are taken into consideration when performing flap design in reconstruction surgery.

This study has several limitations. First, the n value to proceed with deep learning was insufficient. There is a need to further improve the accuracy of the automatic segmentation system by conducting external validation using additional datasets. As aforementioned, the detection accuracy for perforators on the skin was slightly lower, so retraining is necessary by reducing the region of interest (ROI). The ROI set in our study was from the anterior superior iliac crest to directly superior to the patella. It would be helpful to conduct additional study by reducing the ROI based on the ABC system. As manual detection is time-consuming, it seems necessary to evaluate efficiency by comparing the difference in the time required for manual and automatic segmentations.

Nevertheless, this study suggested the clinical applicability of automatic detection of ALT

flap perforator. Additional research may improve the accuracy and efficiency of the automatic detection for anterolateral thigh flap perforators in maxillofacial reconstruction.

# Conclusion

In this study, when automatic segmentation was performed on the ALT flap perforator using 2D and 3D images, DSC and JSC values were derived at reasonable levels. Furthermore, when the perforator was marked as a point on the thigh skin and the distance between the two points was compared, the variation was not prominent. This suggests that automatic segmentation for ALT flap perforators has potential for clinical application.

# References


1. Song Y-g, Chen G-z, Song Y-l. The free thigh flap: a new free flap concept based on the septocutaneous artery. British journal of plastic surgery. 1984;37(2):149-59.
2. Wei F-c, Jain V, Celik N, Chen H-c, Chuang DC-C, Lin C-h. Have we found an ideal soft-tissue flap? An experience with 672 anterolateral thigh flaps. Plastic and reconstructive surgery. 2002;109(7):2219-26.
3. Kimata Y, Uchiyama K, Ebihara S, Sakuraba M, Iida H, Nakatsuka T, et al. Anterolateral thigh flap donor-site complications and morbidity. Plastic and reconstructive surgery. 2000;106(3):584-9.
4. Nasajpour H, Steele MH. Anterolateral thigh free flap for “head-to-toe” reconstruction. Annals of plastic surgery. 2011;66(5):530-3.
5. Ali RS, Bluebond-Langner R, Rodriguez ED, Cheng M-H. The versatility of the anterolateral thigh flap. Plastic and Reconstructive Surgery. 2009;124(6S):e395-e407.
6. Lee Y-C, Chen W-C, Chou T-M, Shieh S-J. Anatomical variability of the anterolateral thigh

flap perforators: vascular anatomy and its clinical implications. Plastic and reconstructive surgery. 2015;135(4):1097-107.

7. Rozen WM, Ashton MW, Pan WR, Kiil BJ, McClure VK, Grinsell D, et al. Anatomical variations in the harvest of anterolateral thigh flap perforators: a cadaveric and clinical study. Microsurgery: Official Journal of the International Microsurgical Society and the European Federation of Societies for Microsurgery. 2009;29(1):16-23.

8. Valdatta L, Tuinder S, Buoro M, Thione A, Faga A, Putz R. Lateral circumflex femoral arterial system and perforators of the anterolateral thigh flap: an anatomic study. Annals of plastic surgery. 2002;49(2):145-50.

9. Choi S-W, Park J-Y, Hur M-S, Park H-D, Kang H-J, Hu K-S, et al. An anatomic assessment on perforators of the lateral circumflex femoral artery for anterolateral thigh flap. Journal of craniofacial surgery. 2007;18(4):866-71.

10. Wong C-H, Wei F-C, Fu B, Chen Y-A, Lin J-Y. Alternative vascular pedicle of the anterolateral thigh flap: the oblique branch of the lateral circumflex femoral artery. Plastic and reconstructive surgery. 2009;123(2):571-7.

11. Gunnarsson GL, Tei T, Thomsen JB. Color Doppler ultrasonography–targeted perforator mapping and angiosome-based flap reconstruction. Annals of Plastic Surgery. 2016;77(4):464-8.

12. Cho M-J, Kwon JG, Pak CJ, Suh HP, Hong JP. The role of duplex ultrasound in microsurgical reconstruction: review and technical considerations. Journal of Reconstructive Microsurgery. 2020;36(07):514-21.

13. Kehrer A, Sachanadani NS, da Silva NPB, Lonic D, Heidekrueger P, Taeger CD, et al. Step-by-step guide to ultrasound-based design of alt flaps by the microsurgeon–basic and advanced applications and device settings. Journal of Plastic, Reconstructive & Aesthetic Surgery. 2020;73(6):1081-90.

14. Cohen OD, Abdou SA, Nolan IT, Saadeh PB. Perforator variability of the anterolateral thigh

flap identified on computed tomographic angiography: anatomic and clinical implications. Journal of Reconstructive Microsurgery. 2020;36(08):616-24.

15. Mavioso C, Araújo RJ, Oliveira HP, Anacleto JC, Vasconcelos MA, Pinto D, et al. Automatic detection of perforators for microsurgical reconstruction. The Breast. 2020;50:19-24.

16. Araujo RJ, Garrido V, Baracas CA, Vasconcelos MA, Mavioso C, Anacleto JC, et al. Computer aided detection of deep inferior epigastric perforators in computed tomography angiography scans. Computerized Medical Imaging and Graphics. 2019;77:101648.

17. Gargeya R, Leng T. Automated identification of diabetic retinopathy using deep learning. Ophthalmology. 2017;124(7):962-9.

18. Valente IRS, Cortez PC, Neto EC, Soares JM, de Albuquerque VHC, Tavares JMR. Automatic 3D pulmonary nodule detection in CT images: a survey. Computer methods and programs in biomedicine. 2016;124:91-107.

19. Khor K-C, Ting C-Y, Phon-Amnuaisuk S. A cascaded classifier approach for improving detection rates on rare attack categories in network intrusion detection. Applied Intelligence. 2012;36:320-9.

20. Wu L, Xin Y, Li S, Wang T, Heng P-A, Ni D, editors. Cascaded fully convolutional networks for automatic prenatal ultrasound image segmentation. 2017 IEEE 14th international symposium on biomedical imaging (ISBI 2017); 2017: IEEE.

21. Weber M, Wang H, Qiao S, Xie J, Collins MD, Zhu Y, et al. Deeplab2: A tensorflow library for deep labeling. arXiv preprint arXiv:210609748. 2021.

22. He K, Zhang X, Ren S, Sun J, editors. Deep residual learning for image recognition. Proceedings of the IEEE conference on computer vision and pattern recognition; 2016.

23. Reenadevi R, Sathiya T, Sathiyabhama B. Breast cancer histopathological image classification using augmentation based on optimized deep ResNet-152 structure. Annals of the Romanian Society for Cell Biology. 2021;25(6):5866-74.

24. Sherer MV, Lin D, Elguindi S, Duke S, Tan L-T, Cacicedo J, et al. Metrics to evaluate the

performance of auto-segmentation for radiation treatment planning: A critical review. Radiotherapy and Oncology. 2021;160:185-91.

25. Organization WH. Obesity: preventing and managing the global epidemic: report of a WHO consultation. 2000;894:9.

26. Kimata Y, Uchiyama K, Ebihara S, Nakatsuka T, Harii K. Anatomic variations and technical problems of the anterolateral thigh flap: a report of 74 cases. Plastic and Reconstructive Surgery. 1998;102(5):1517-25.

27. Wei Y, Feng J, Liang X, Cheng M-M, Zhao Y, Yan S, editors. Object region mining with adversarial erasing: A simple classification to semantic segmentation approach. Proceedings of the IEEE conference on computer vision and pattern recognition; 2017;1568-1576.

28. Park T, Liu M-Y, Wang T-C, Zhu J-Y, editors. Semantic image synthesis with spatially-adaptive normalization. Proceedings of the IEEE/CVF conference on computer vision and pattern recognition; 2019;2337-2346.

29. Illg C, Krauss S, Rachunek K, Hoffmann S, Denzinger M, Kolbenschlag J, et al. Does leg dominance influence anterolateral thigh flap perforators? Microsurgery. 2022;42(8):817-23.

30. Rawat W, Wang Z. Deep convolutional neural networks for image classification: A comprehensive review. Neural computation. 2017;29(9):2352-449.

31. Karpathy A, Fei-Fei L, editors. Deep visual-semantic alignments for generating image descriptions. Proceedings of the IEEE conference on computer vision and pattern recognition; 2015;3128-3137.

32. Zhao Z-Q, Zheng P, Xu S-t, Wu X. Object detection with deep learning: A review. IEEE transactions on neural networks and learning systems. 2019;30(11):3212-32.

33. Zettler N, Mastmeyer A. Comparison of 2D vs. 3D U-Net Organ Segmentation in abdominal 3D CT images. arXiv preprint arXiv:210704062. 2021.

34. Strzelecki M, Szczypinski P, Materka A, Klepaczko A. A software tool for automatic classification and segmentation of 2D/3D medical images. Nuclear instruments and methods

in physics research section A: Accelerators, Spectrometers, Detectors and associated equipment. 2013;702:137-40.

35. Li M, Chen Y, Ji Z, Xie K, Yuan S, Chen Q, et al. Image projection network: 3D to 2D image segmentation in OCTA images. IEEE Transactions on Medical Imaging. 2020;39(11):3343-54.

36. Nguyen DT, Hua B-S, Yu L-F, Yeung S-K. A robust 3d-2d interactive tool for scene segmentation and annotation. IEEE transactions on visualization and computer graphics. 2017;24(12):3005-18.

37. Yu P, Youssef A. Efficacy of the handheld Doppler in preoperative identification of the cutaneous perforators in the anterolateral thigh flap. Plastic and reconstructive surgery. 2006;118(4):928-33.

# List of tables

**Table 1. Progression type of perforators according to gender**

| N(%) | | Septocutaneous | | Musculocutaneous | | |
|---|---|---|---|---|---|---|
| | | Lt. | Rt. | Lt. | Rt. | Total |
| Training | Male | 21(38.9) | 19(35.2) | 6(11.1) | 8(14.8) | 54 |
| | Female | 11(19.0) | 13(22.4) | 18(31.0) | 16(27.6) | 58 |
| | Total | 32(28.6) | 32(28.6) | 24(21.4) | 24(21.4) | 112 |
| Validation | Male | 6(30.0) | 6(30.0) | 4(20.0) | 4(20.0) | 20 |
| | Female | 1(16.7) | 1(16.7) | 2(33.3) | 2(33.3) | 6 |
| | Total | 7(26.9) | 7(26.9) | 6(23.1) | 6(23.1) | 26 |

**Table 2. Dice Similarity Coefficient and Jaccard Similarity Coefficient values of automatic segmentation for lateral circumflex femoral artery perforators**

| Mean (%) ± SD | Training and validation | Test |
|---|---|---|
| DSC | 69.67 ± 1.48 | 69.34 ± 0.83 |
| JSC | 67.81 ± 1.70 | 67.47 ± 0.96 |

SD: standard deviation, DSC: dice similarity coefficient, JSC: jaccard similarity coefficient

**Table 3. Comparison of DSC and JSC values according to gender, left and right thighs, perforator progression type, and BMI**

| Mean(SD) | | DSC | JSC |
|---|---|---|---|
| Gender† | | | |
| | Female | 68.78(1.18) | 66.72(0.67) |
| | Male | 69.51(0.69) | 67.70(0.94) |
| | *p* value | 0.287 | 0.112 |
| Location† | | | |
| | Left | 69.73(1.64) | 68.95(1.69) |
| | Right | 67.82(1.58) | 67.14(1.89) |
| | *p* value | 0.005* | 0.026* |
| Perforator progression† | | | |
| | Septocutaneous | 69.33(1.58) | 67.18(1.93) |
| | Musculocutaneous | 69.36(1.85) | 67.84(1.49) |
| | *p* value | 0.86 | 0.297 |
| BMI‡ | | | |
| | Healthy weight (18.5–24.99 kg/m2) | 69.27(0.91) | 67.31(0.99) |
| | Overweight (25–29.99 kg/m2) | 69.82(0.58) | 68.19(0.90) |
| | Obese (≥30 kg). /m2) | 69.04(0.00) | 67.60(0.00) |
| | *p* value | 0.459 | 0.392 |

*: statistically significant with $p < 0.05$, †: Mann-Whitney u-test, ‡: Kruskal-Wallis test

SD: standard deviation, DSC: dice similarity coefficient, JSC: jaccard similarity coefficient, BMI: body mass index

# List of figures

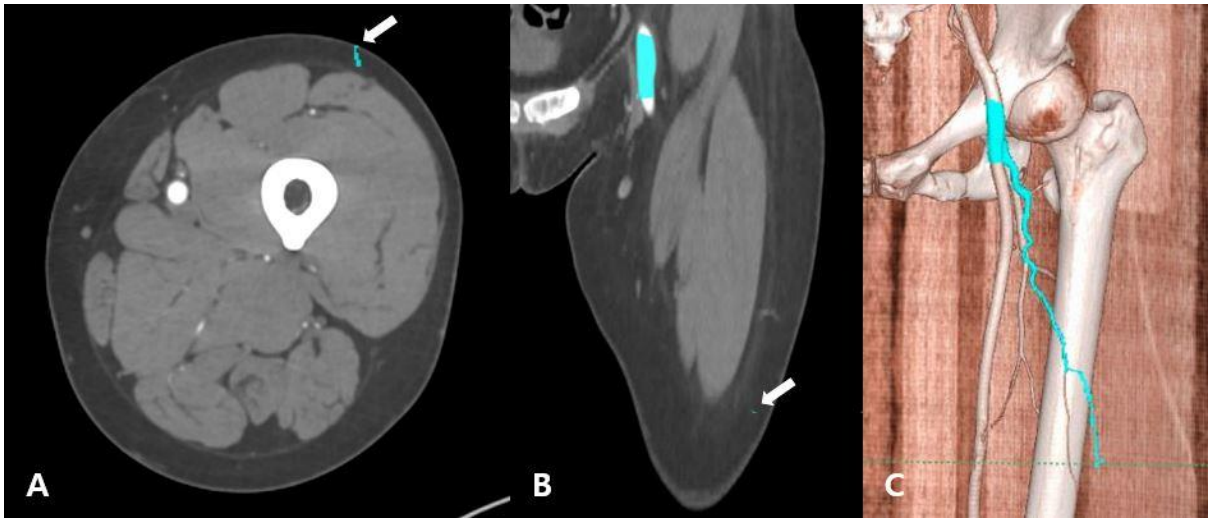


Figure 1. Axial (A), coronal (B), and 3D (C) views of computed tomography angiography. Manual mapping from the femoral artery near the hip joint to the lateral circumflex femoral artery perforator was performed continuously to the terminal point reaching the thigh skin.

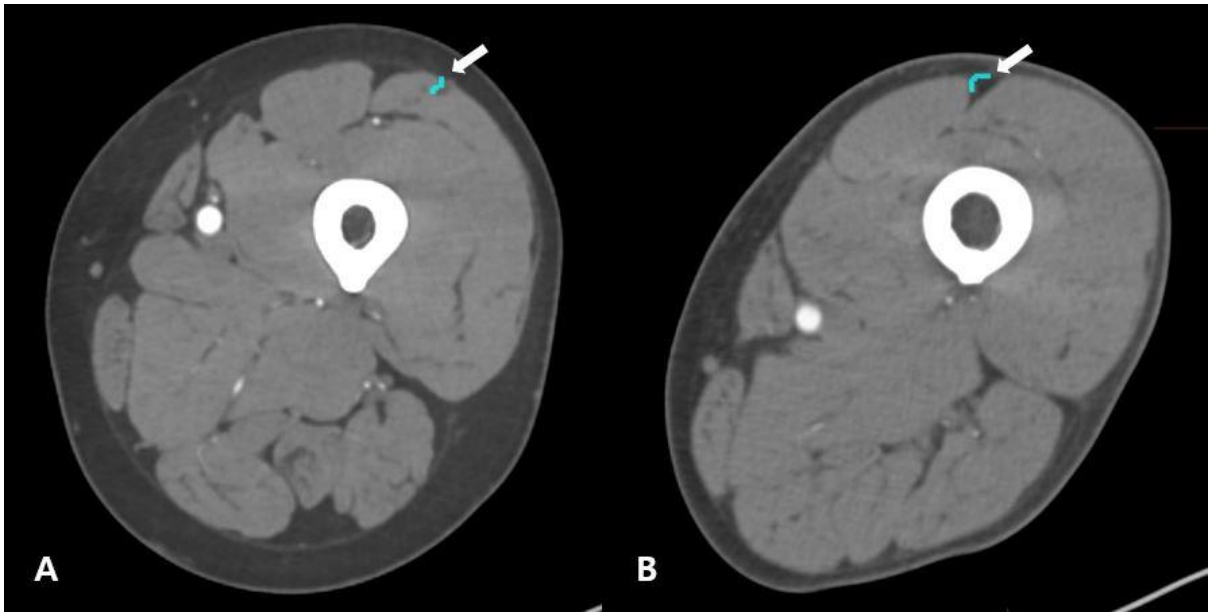


Figure 2. The axial views show the perforator progression as musculocutaneous (A) and septocutaneous (B).

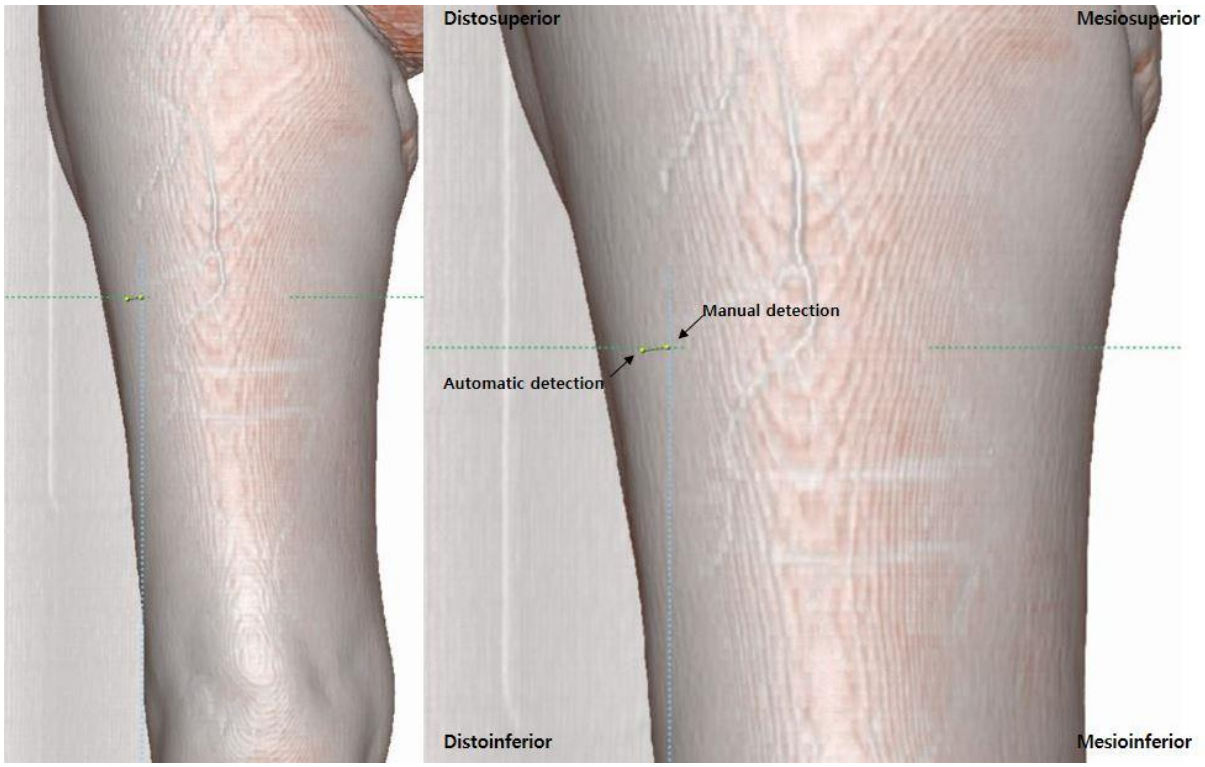


Figure 3. After superimposing manually and automatically segmented perforators on the thigh skin, the difference in the coordinate values between two points was calculated.

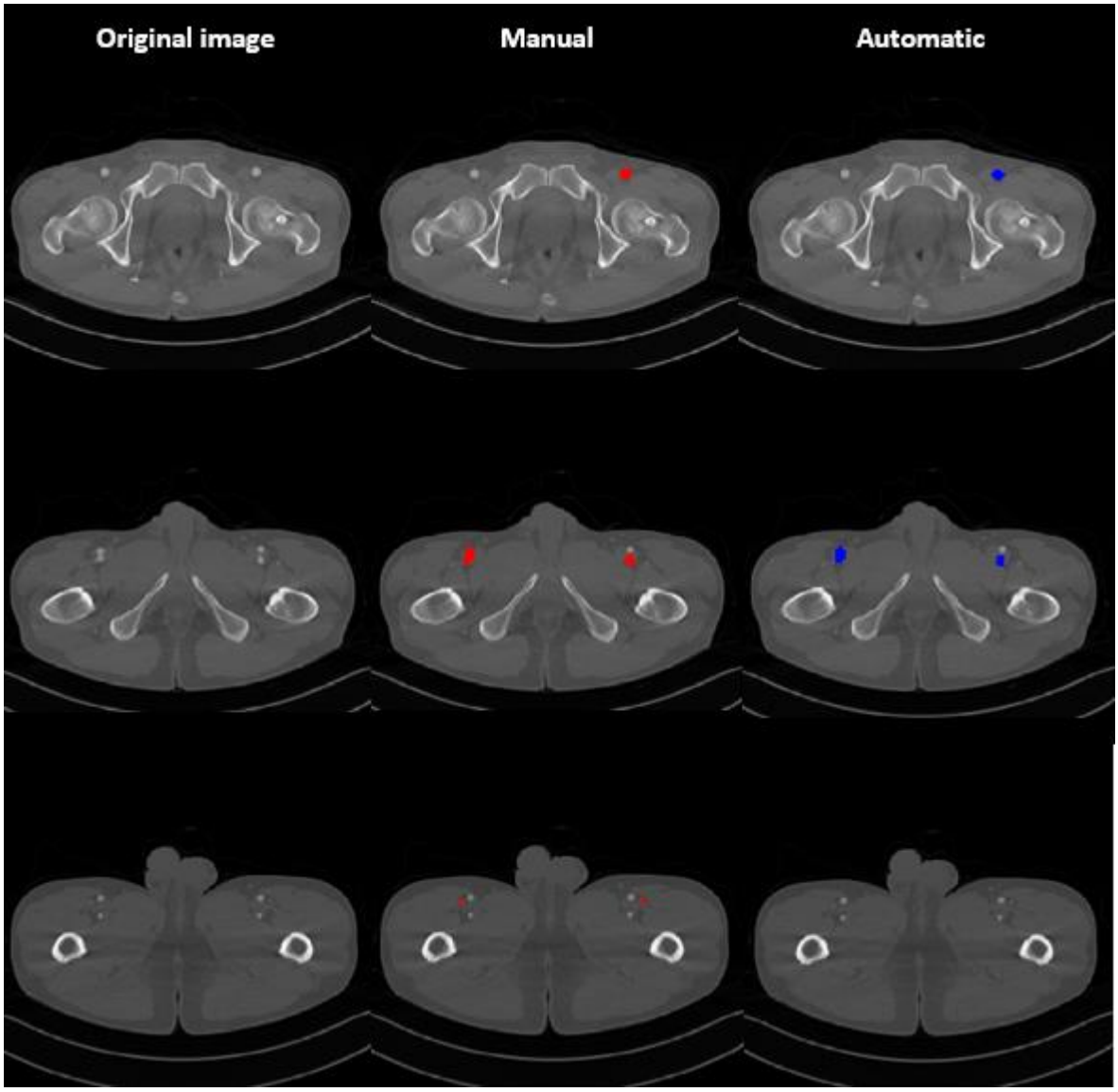


Figure 4. Axial images of original, manual, and automatic detections. The results of the manual and automatic detections showed similarity. As the diameter of arteries got smaller, discontinued portions were confirmed.

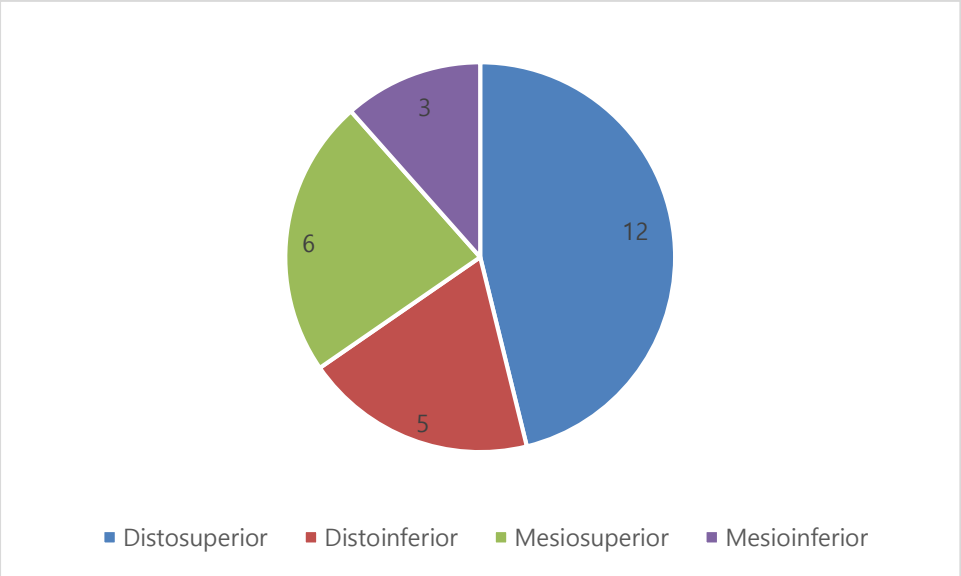


Figure 5. Quadrant distribution of the automatic perforator detection.

국문 요약

# 두경부 재건에서 인공지능을 이용한 전외측대퇴피판 천공기의 자동감지 시스템 개발

오지수

지도교수 이지호

울산대학교 대학원 의학과 치의학전공

**개요**

전외측대퇴피판은 악안면 재건에서 선호되는 피판 중 하나이며 그것의 피부 천공기를 찾는 것이 피판 디자인 수립의 중요한 첫번째 단계이다. 컴퓨터 단층촬영 혈관조영술은 이미지 매핑을 통해 피판 천공기 감지에 활용된다. 그러나, 술전 매핑을 시간이 소요되고 영상의 질과 임상가의 숙련도에 영향을 받는다. 본 연구는 합성곱 신경망을 이용하여 컴퓨터 단층촬영 혈관조영술 상에서 전외측대퇴피판 천공기의 자동 감지 시스템을 개발하고 그것의 효율성과 정확성을 평가하는 것을 목표로 한다.

**재료 및 방법**

악안면 재건을 위해 CTA 를 시행한 총 80 명의 대상자를 수집하였다. 한 명의 연구자가 AVIEW Modeler 소프트웨어(버전 1.1.42.7, Coreline Software, 서울, 한국)를 사용하여 업로드된 CTA 에서 양측 대퇴 회선동맥 천공기 매핑을 수행하였다. 자동 감지 시스템 개발을 위한 트레이닝은 DeepLabv2 및 3D ResNet152 를 사용하였다. 주사위 유사성 계수(DSC)와 Jaccard 유사성 계수(JSC) 값을 계산하고, 두 지점 사이의 거리 차이와 사분면 분포 분석을 수행하였다.

**결과**

DSC 값은 69.67±1.48, JSC 값은 67.81±1.70 으로 나타났다. 13 명의 dataset 에 대한 test 결과는 DSC 69.34 ± 0.83, JSC 67.47 ± 0.96 로 나왔다. 수동감지과 자동감지의 거리 차이는 좌측이 각각 38.28 ± 15.52 mm, 우측이 31.96 ± 18.11 mm 이었다. 사분면 분포는 distosuperior 영역에 가장 많이 나타났다.

**결론**

도출된 결과값을 바탕으로 했을때, 전외측대퇴피판 천공기의 자동 감지 시스템은

임상 적용 가능성을 고려할 수 있다.

중심어: 전외측대퇴피판, 천공기, 자동 분할, 영상 매핑